Obtaining Minimum Energy Biped Walking Gaits with Symbolic Models and Numerical Optimal Control

M. Hardt[1] K. Kreutz-Delgado[2] J.W. Helton[3] O. von Stryk[1]

[1] *Zentrum Mathematik, Techn. Univ. München, D-80290 München, Germany*
[2] *Dept. of Elec. Eng., UCSD, 9500 Gilman Dr., La Jolla, CA 92093-0407, U.S.A.*
[3] *Dept. of Math., UCSD, 9500 Gilman Dr., La Jolla, CA 92093-0112, U.S.A.*

We discuss our solution to the problem of generating symmetric, periodic gaits for a 5-link biped robot. We seek to approximate natural motion through the minimization of its injected energy. Our model stands out in that we consider the complete nonlinear dynamical model for the robot moving in the sagittal plane of forward motion. Both phases of walking, the swing and double-support phases, are explicitly modeled, including the contact and collision effects characteristic of each phase. A large number of constraints involving the contact forces, conditions for periodicity, and the range of motion must be considered which ensure the validity of the calculated motion. The solution of this complex problem was made possible through the use of various symbolic, dynamical algorithms relating to multibody systems in combination with powerful numerical optimal control software. Recent improvements in both areas have also further increased the potential to treat even more complex biped models. The symbolic nature of the recursive multibody algorithms, used for evaluating the dynamics and influences of contact and collision, facilitate any changes made to the number of limbs, points of actuation, or to the mass and inertia properties of the system. This flexibility allows one to readily treat many different cases such as the underactuated case when no ankle torques are allowed, and the introduction of impulsive forces for control purposes. The minimum energy walking problem becomes a path planning problem on a 14-dimensional state space with saturation and algebraic constraints on the state variables. The solution will satisfy a Hamilton-Jacobi-Bellman type equation along the optimal path. The optimal control software DIRCOL may solve such multi-phase problems with various forms of constraints, and it handles well the high degree of nonlinearity and dimensionality found in our problem. A newly available version of this software has also provided a substantial decrease in the required computing time for generating solutions. We discuss these and other improvements to our solution approach in this paper.

1 Introduction

Modeling and understanding the seemingly simple process of human walking remains as one of the more difficult research problems in multibody systems and robotics due to its complexity and high dimension. There are many variations of walking in humans, though we will concern ourselves only with the periodic motion associated with moving at a constant average speed on a flat surface. Due to the complexity of the problem, compromising simplifying modeling assumptions were often made in previous work to make it more tractable. Even a simple 5-link biped robot with all rotational joints and full motion degrees of freedom will have a 14 dimensional state space when represented with respect to generalized coordinates. One also encounters a differential-algebraic system when contact constraints of the leg with the ground are considered.

A very thorough investigation into minimum energy walking with numerical methods was undertaken early on in [2] using a highly simplified model which resulted in a 2-link manipulator. The idea of searching for a passive walking motion which can approximate better the minimum energy motion witnessed in humans was also expressed in the work of McGeer [9] and later with Goswami et al. [5]. The minimum energy path is desirable for it exhibits stabilizing, attractive properties. Our experiments have shown that many walking trajectories, naively chosen to approximate walking motion, can require a huge increase in energy over that of the

1

optimally calculated minimum energy motion. Other recent work also investigating minimum energy motion with simplified models may be found in [11]. Very interesting walking machines were constructed by McGeer [9] and also by Kajita [8]. Kajita modeled the biped dynamics as an inverted pendulum with point masses whose simplicity forced an interesting and unusual construction of the biped.

To properly model walking, one should consider explicitly both phases of walking. The first phase has one leg in contact, while in the shorter second phase both legs are in contact with the ground. The difficulty with this perspective, however, is that one is faced with a differential-algebraic system with a varying number of algebraic constraints. The collision of the leg with the ground results in jump conditions on the velocities while there also exists saturation constraints on the state variables and the actuators.

In this paper, we explain how our numerical approach is able to produce solutions which satisfy these and other constraints. The first step towards reducing the complexity of the problem was made in modeling the dynamical system very efficiently using recently developed recursive, symbolic algorithms [6]. This allows one to change the model "easily" and to greatly speed (the very many) function evaluations which occur in running an optimization code (or even a simulation). This is described in [6] and in this paper we briefly sketch how recursive symbolic dynamics are used on the biped.

Another important step was the creation of a reduced dynamics algorithm for evaluating the unconstrained reduced-dimensional dynamics of the biped which account for the contact constraints [7]. This makes it possible to integrate in time the reduced system rather than the full differential-algebraic dynamical system. This algorithm was first presented in the description of this work found in [7].

The last component of our solution approach involves the use of powerful numerical optimal control software (DIRCOL) [14, 15, 16]. This recently developed software can handle control problems of high dimension with many forms of constraints. We describe how we successfully apply these calculational tools to our problem. Our description includes coordinate selections which proved essential for ours and possibly for other numerical approaches, see Section 3.5. We also indicate numerical experience with the use of DIRCOL in Section 5.1.

We finally discuss our experimental findings and compare a few of them to medical findings on humans. Noteworthy are:

• Minimum energy walk for biped model (without explicit modeling of the feet) has a much slower walk than the optimal human walk.

• The optimal model walk has shorter steps than the optimal human walk; however, step length comparisons with the human walk are difficult because our model has no feet. These findings suggest an area for future work.

• The curve "energy of optimal walk (resp. optimal step length) vs average forward velocity," which we obtained numerically, has the same qualitative shape as the hyperbolic (resp. linearly) relationship clinically observed in humans.

In an attempt to add actuation which might resemble the action of feet we included two forces. First we allowed an additional liftoff force which acts as an impulse directed upward on the bottom of the swing leg when it lifts off of the ground. This resembles the upward thrust imparted by the foot at liftoff. Secondly, we allowed ankle torques at the point of contact of the legs with the ground.

In the discussion of our numerical experiments, we studied many different model variations and present here a few of them. For example, we turn the liftoff impulse and ankle torques on and off. Other parameters which are varied are the biped's step length, the time of one step, and the proportion of time corresponding to the contact phase. We also discuss the effect of these parameters on the system energy. Findings on the liftoff impulse and the ankle torques are:

2

• Impulsive liftoff forces help prevent torque saturation, smooth the walking motion, and reduce the energy consumed.

• Ankle actuation smooths the walking step and distributes the required input torques more equally among the hip, the knee, and the ankle.

Preliminary results for the solution of this problem were first presented in [7] while the whole paper is based on [6].

2 Human Walking

The human walking step is composed of two different phases. The first phase is the *swing phase* or single support phase when one foot is on the ground while the other swings. This phase begins with the *moment of liftoff* and ends with the *collision* of the swing foot with the ground. This phase makes up the majority $(80 - 90\%)$ of the duration of the walking step in human walking. The second phase is called the *double support phase* as both feet are on the ground while the body is moving forward. This phase usually makes up only a small part $(10 - 20\%)$ of the human walking step.
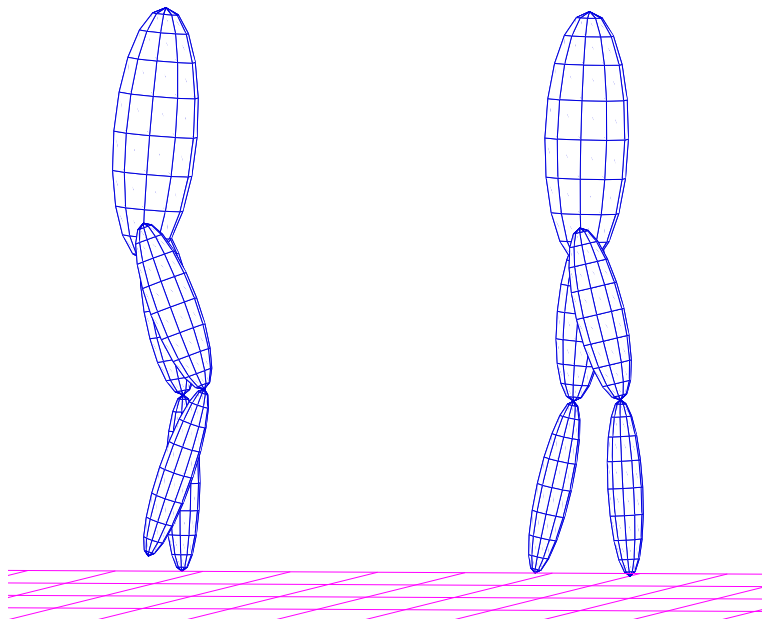

Figure 1: Walking Phases

Also of interest are the transitions between phases. Immediately at the beginning of the swing phase is the *moment of liftoff*. Here, the foot is just propelling the body forward so that the leg loses contact with the ground. The other transition between the swing and double support phases is characterized by a *collision* of the swing foot with the ground. **Figure 1** gives a graphical depiction of our biped model first in the swing phase, then in the double support phase.

Some additional detailed definitions can be useful. The *cadence* is defined as the number of steps in a standard time frame (e.g. steps/min). The *step length* is the distance between the same point on each foot during the double support phase. The *stride length*, on the other hand, is the distance traveled between two successive foot strikes of the same foot and is equal

3

to two step lengths. Each stride is, thus, composed of one right and one left step length. All measurements given will be in meters.

3 Model and Dynamics

3.1 Biped Model

Many of the essential characteristics of the human walking motion may be captured with a 5-link planar biped walking in the two-dimensional sagittal plane, the vertical plane bisecting the front of the biped. The model contains two links for each leg plus a large, massive torso, which also functions as the base of the tree-structured multibody system. Though the motion is constrained to the 2-dimensional vertical sagittal plane, in our experiments we model the links with a 3-dimensional elliptical shape and a uniform distribution of mass. The physical data corresponding to the model used in our experiments can be found in Table 1.

Table 1: Biped Model Physical Data

Link	Mass	Length	Radius
Torso	20 kg	0.72 m	0.12 m
Upper Leg	7 kg	0.50 m	0.07 m
Lower Leg	4 kg	0.50 m	0.05 m

Though feet are not included in our biped model, much of their influence may be modeled in ways which do not increase the dimension of the system. From the control perspective, two of the main contributions of the feet, when not expressly considering friction, are the introduction of ankle torques and the liftoff force produced as the heel comes off of the ground. It is possible to include ankle torques in the model by treating these as external forces influencing the tips of each leg at the points of contact. Rather than modeling a liftoff force which lasts the entire duration of the double contact phase, as is normally the case with the foot, we model the liftoff force as an instantaneous impulsive force occurring at the moment of liftoff. This last technique has certain numerical advantages though it cannot completely reproduce the effect of the foot as will be shown in the reports of our numerical experiments.

There are a total of 14 states, 6 control variables, and 1 control parameter in our control problem if an impulse liftoff force is modeled.

x_1–x_3 torso orientation and position in the vertical plane
x_4–x_6 torso angular and linear velocity
x_7,x_8 angle position and velocity of leg 1 hip
x_9,x_{10} angle position and velocity of leg 1 knee
x_{11},x_{12} angle position and velocity of leg 2 hip
x_{13},x_{14} angle position and velocity of leg 2 knee
u_1,u_2 applied torque at leg 1 hip and knee
u_3,u_4 applied torque at leg 2 hip and knee
u_5,u_6 applied torque at leg 1 & 2 ankles

3.2 Recursive, Symbolic Dynamical Algorithms

The state equations of the biped walker are those of a multibody system experiencing contact forces,

$$\ddot{\theta} = \mathcal{M}^{-1}(u + J_c^T f_c - \mathcal{C} - \mathcal{G}) \ . \tag{1}$$
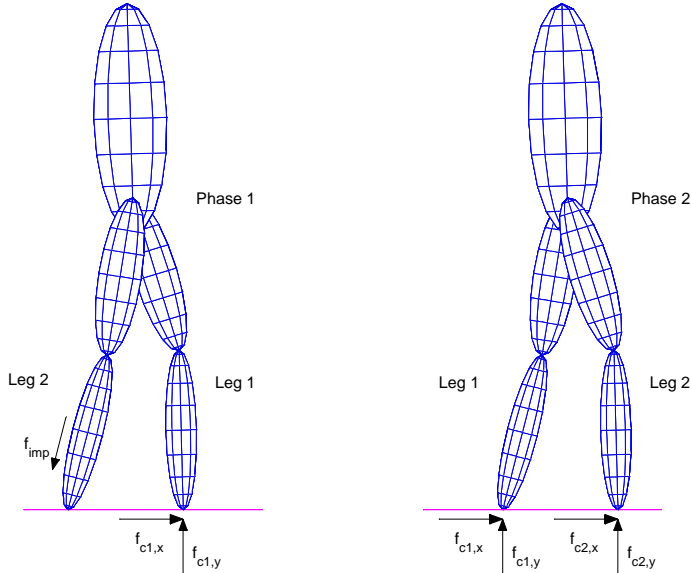
4

Figure 2: At the beginning of phase 1 an impulse force f_{imp} can propel the body forward. During phase 2, both legs experience contact forces.

In equation (1), $\mathcal{M}$ is the square, positive-definite mass-inertia matrix, $\mathcal{C}$ is the vector of Coriolis and centrifugal forces, $\mathcal{G}$ is a vector of gravitational forces, u are the applied torques at the links, J_c is the constraint Jacobian, and f_c is the constraint force.

Several different approaches to recursive, symbolic multibody algorithms were studied, compared, and represented in a unifying formalism in [6]. This work also included the extension of several algorithms to multiple degree of freedom joints and tree-structured systems. The approach is based on decomposing the dynamical quantities into physical, matrix operators. The various link operations are stacked into larger, matrix operators which, in turn, provide a very clean notation which can easily be manipulated for estimation and control design purposes. For high dimensions, recursive, symbolic dynamical models are more efficient for calculating the forward dynamics than other non-recursive procedures which require constructing and inverting the entire mass-inertia matrix, $\mathcal{M}$.

3.3 Contact and Reduced Dynamics

Special recursive algorithms have also been developed to determine the contact forces experienced by the biped under contact and the resulting generalized accelerations $\ddot{\theta}$ which are produced. See Appendix 1, also see [7] and the references found therein.

An important component of our dynamical modeling which also contributed to our ability to solve this problem was the development of a Reduced Dynamics Algorithm which makes use of the Contact Algorithm and which is more fully described in Appendix 2. Because of the contact constraints, we are faced with a differential-algebraic system. Two courses of actions are possible when it is necessary to integrate the dynamics, one being the use of specially tailored integration routines which often require the partial derivatives of the various contact constraints. The preferable approach, however, is to use a reduced unconstrained set of dynamics which evolve on the constraint manifold. Then it is possible to use standard integration procedures. This latter approach is the one we take.

In the first phase of the biped motion, where one leg is swinging, the contact constraints reduce the total degrees of freedom from 7 to 5. Thus, using the Reduced Dynamics Algorithm, an unconstrained 10-dimensional state space can represent the system during this period instead of the full 14 dimensions for the completely free system. The remaining 4 states and their time derivatives can be determined from the 10 independent states and their time derivatives. Similarly in the shorter second phase, when both feet are in contact with the ground, contact constraints allows us to work with a system with only a 6-dimensional state space.

3.4 Collision and Impulsive Forces

Closely related to the Contact Algorithm is the Collision Algorithm. This algorithm calculates the discontinuous jump in generalized velocities resulting from inelastic collisions of the multibody system with its environment. We model the collision of the swing leg as it makes contact with the ground in this manner. The recursive algorithm determines first the instantaneous impulsive force experienced by the system, then propagates it throughout all the links of the multibody system.

In several of our experiments, we *introduce* an impulsive force along the axis of the leg about to lift off of the ground thereby aiding the biped in maintaining its forward momentum. The Collision Algorithm can also be used to determine the resulting jump in the generalized velocities. The magnitude of the impulsive force becomes an additional control parameter which must be included into the energy criteria to be discussed in Section 4. **Figure 2** displays both the influence of the contact forces on the biped model and the introduction of an impulsive liftoff force.

3.5 Box Constraints and Polar Position Coordinates

Magnitude constraints on the state, control, and parameter variables, such as those arising from saturation constraints, translate mathematically to simple inequality constraints on individual variables. Such constraints are typically called *box constraints*. Numerically, these usually are the most tractable type of inequality constraints, making it preferable to put constraints in box form whenever possible. Much worse are inequality constraints on nonlinear functions of the states, controls, and parameters.

It is desirable to find, if possible, a change of coordinates to reformulate a nonlinear inequality constraint as a simple box constraint with a different set of variables. This simple trick turns out to be very important for dealing with a key constraint in our biped motion problem, namely, that *the length of the leg on the ground and the hip height are compatible.* In Cartesian coordinates, this translates to a nonlinear inequality constraint which, if implemented directly, has numerically unpleasant consequences. Indeed, we were unable to solve biped optimal path planning problems until we realized that by using polar coordinates the hip vs. leg length constraint becomes equivalent to a collection of box constraints.

We give here more details on this and other box constraints. Recall that there exist two position variables describing the x and y position coordinates for the torso and, consequently, the entire biped robot. These position coordinates are represented in the local torso coordinate system. The nonlinear inequality constraints which we mentioned above is that the hip remain at a distance from the origin no greater than the length of an extended leg. This requirement affects leg 1 which supports the body during the swing phase. With the use of the Reduced Dynamics Algorithm, the position and velocity variables for leg 1 are not part of the state used in the optimization process. Their values must be calculated via inverse kinematics and the Collision Algorithm every time the dynamics need to be evaluated. If the hip is too far from the origin, then we will not have sufficient information to determine the state of leg 1

plus the system will have entered a free-flying configuration during phase 1 or a single-support configuration during the double support phase. By converting the x, y coordinates to polar coordinates r and θ, it is then possible to place a simple magnitude constraint on r which will serve the same function as the nonlinear inequality constraint previously mentioned.

Additional box constraints on the state variables correspond to ensuring a sensible range of motion for the robot such as that the knee may not bend backwards. We place magnitude box constraints as well on the applied torques at the hip, knee, and ankle. We will describe in the experiment section how these constraints become active while moving at higher velocities and how impulsive liftoff force can partially remedy the problem. The bounds we place on the ankle torques are only half of those at the hip and knees.

3.6   Boundary Constraints

As we are solving a finite-time problem, the boundary constraints of the biped walking problem represent an important part of the problem definition. We allow a number of parameters to be variable. These are as follows:

$$
\begin{aligned}
p_1 &= \text{\textit{step length (meters)}} \\
p_2 &= \text{\textit{magnitude of liftoff impulsive force}} \\
p_3 &= \text{\textit{time of collision (seconds)}} \\
p_4 &= \text{\textit{average forward velocity (meters/min)}}
\end{aligned}
$$

At the initial and final time, periodicity of the states and controls must be enforced while in between phases continuity is enforced. Another boundary constraint is that if an impulsive liftoff force is included at the beginning of phase 1, then the velocities must reflect the sudden jump caused by the impulsive force. Given the magnitude of the impulsive force p_2, the Collision Algorithm can determine the resulting new velocities for the beginning of phase 1. A further boundary constraint is the swing leg must also land at the time of collision, p_3, at a step size equal to p_1. Since in our experiments we constrain the proportion of phase 1 to 85% of the total time of the walking step, the final or total time (also variable) may be determined from the phase 1 duration p_3.

3.7   Nonlinear Inequality Contraints

There are several constraints which must be enforced along the duration of the walking step. First, we must ensure that the swing leg always remain above ground while in motion during phase 1. This involves a series of simple kinematic calculations. Additionally, we require that the vertical component of the contact forces in each phase remain positive so that there is not a premature liftoff of the leg from the ground. If this component does not remain positive and we are still constraining the leg to be in contact, then the configuration will not make sense.

These contact constraints do require a significant amount of computation in order to evaluate them, and we have determined them to be necessary as they can easily be violated if they are left out. In fact, the necessity of these constraints inspired us to begin working with a more complex tree-structured model with the torso as the base of the biped and full positional degrees of freedom in the plane. A simpler model would take the foot which is always in contact with the ground during one step to be the base. Several investigators take this approach in their handling of the problem, but this prevents the verification of the contact force inequalities.

4 Minimum Energy Performance

Experiments have shown humans to walk in an energy efficient manner. In [10], a detailed study is presented of energy expenditure in actual human walking where researchers have explored the relationships which exist between real energy data and human walking motion. A simple yet fairly accurate relationship is one in which the energy expended is quadratic in the forward velocity,

$$E_w = 32 + 0.005v^2 \ . \tag{2}$$

Here v is the average forward velocity in m/min and E_m is the energy requirement in $cal/kg/min$ for the average human subject. An often more desirable set of units for walking energy is to measure it per distance traveled (m = meters) rather than per time elapsed (min = minutes) since this conveys more the notion of energy economy. We denote this form of energy as E_m. Its units are $cal/kg/m$, and it is related to E_w and the previous relationship by

$$E_m = \frac{E_w}{v} = \frac{32}{v} + 0.005v \ . \tag{3}$$

This function will now have a hyperbolic shape. This and most other functional relationships such as (3) indicate a minimum energy motion of an 80 m/min walking velocity with an energy expenditure of 0.8 $cal/kg/m$. The experiments also show average cadences of 105 $steps/min$ and an average step length of 0.75 m for an adult male.

In our study, we shall minimize a quantity proportional to the injected energy into the system, the integral of the applied torques,

$$J = \Big(\int_0^{T_1} u^T u \, dt + \int_{T_1}^{T} u^T u \, dt \Big) / step \ length \ , \tag{4}$$

where T_1 is the time at the end of the first phase (swing phase), and T is the time at the end of the second phase (double-contact phase). Dividing by the step length, the distance between successive heel strikes, gives the expended energy per meter traveled. If an impulsive force is added, then this control parameter will also be added into the performance,

$$J = \Big(\int_0^{T_1} u^T u \, dt + \int_{T_1}^{T} u^T u \, dt + u_{imp}^2 \Big) / step \ length. \tag{5}$$

This general form of minimal energy performance was also used in [11].

The performance J is not a measure of the mechanical work performed on the system, and we are unable to determine the change in energy of the body from J. In fact, for our biped model, we are minimizing a quantity proportional to the energy required for a motion. In humans, this is analogous to the difference between mechanical energy and metabolic energy. As no system, not even a human, is perfectly efficient, these quantities will differ and their relationship in humans still remains a very difficult and unanswered problem [10]. In robotics, we do not have metabolic energy, but for a simple actuation model, our approach amounts to minimizing the energy required for direct drive motors at the joints to produce the required torques. This approach provides a more numerically tractable way of reaching our performance objectives.

5 Numerical Optimal Control

Direct optimization methods for optimal control are characterized by the minimization of a cost functional which is a function of the system state and the control input u. An example

of such a method is the program DIRCOL [14, 15, 16], which can handle implicit or explicit boundary conditions, arbitrary nonlinear equality and inequality constraints on the state variables, and multiple phases where each phase may contain a different set of state equations. DIRCOL functions by packaging the optimal control problem along with its constraints into a constrained, nonlinear minimization problem which is solved by an SQP-based optimization code NPSOL [3], or SNOPT [4] which takes advantage of sparsity.

The output of the numerical optimal control program will be the optimal open-loop solution for the control $u(t)$ and the corresponding state trajectory $x(t)$ at the choice of grid points in time. DIRCOL discretizes the state and control variables in time over the trajectory. The fineness or coarseness of the discretization can have a large influence over the time required to generate a solution. The recently released DIRCOL 2.0 using sparse optimization techniques has shown itself to be faster and more robust.

As previously mentioned, there are a total of 14 states, 6 control variables, and 1 control parameter in our control problem. All of these quantities have magnitude saturation bounds placed upon them in the optimization process, though the majority never become active. The control saturations are the most important as in many experiments these will saturate, particularly at higher speeds. The bounds on the ankle torques are also smaller than those at the other joints, as the ankles cannot provide as great a force as the hips and knees can.

In addition to magnitude constraints, there are explicit constraints on the initial and final state of each phase which assign those constrained states and controls a fixed value which may depend on other known values. These are called explicit boundary conditions, while implicit boundary conditions are those for which the states and controls must satisfy a nonlinear algebraic equation. Finally, we have nonlinear inequality constraints which must be satisfied by the states and controls along the duration of the walking step. The constraints outlined in Section 3.6 result in a total of:

Explicit boundary conditions at initial and final time: 13
Explicit boundary conditions in between phases: 17
Implicit boundary conditions at initial and final time: 7
Implicit boundary conditions in between phases: 3
Nonlinear Inequality Constraints in phase 1:   2
Nonlinear Inequality Constraints in phase 2:   3

5.1   Optimization Trials

The high degree of nonlinearity and high dimension of the problem, along with all the constraints, make it unreasonable to assume that by specifying the state equations, boundary conditions, and inequality constraints together with a naive initial guess of the solution, the optimization procedure will immediately find an optimal solution. Various simpler problems were first solved such as that of standing in place and then moving only small distances. In fact, an iterated process was undertaken which gradually approximated the actual problem, whereby the solution of each generalization of the problem was made using the previous one as an initialization.

For most trial runs, we used 13 grid points in time, 8 in the first phase and 5 in the second phase. As the number of grid points has a large influence on the length of each optimization run, it is preferable to use a coarse grid, then to refine the grid if more exact solutions are needed. Run times depend on the starting values given to the problem and the problem to be solved.

DIRCOL transforms the complete problem to a nonlinear optimization problem with 197 variables, 131 nonlinear equality constraints, and 23 inequality constraints. The number of function calls during a sample optimization run are:

DIRCOL Version	1.2	2.0
Optimization Program	NPSOL	SNOPT
Function Calls		
State equations	568635	230952
Implicit Boundary Const.	43430	8497
Nonlinear Ineq. Const.	249928	125099
Run Time	18 min.	12 min.

These runs were conducted on a Sparc Ultra 2 with a 166 MHz processor. The advantage of DIRCOL 2.0 over DIRCOL 1.2 in solving a particular problem was, in fact, much greater than the statistics above indicated. This is because several subproblems would often have to be solved with DIRCOL 1.2 before the complete problem could be solved. For example, a subproblem would be solved without enforcing positivity of the contact constraints, then the complete problem could be solved by initializing it on the solution of the subproblem. DIRCOL 2.0 would usually not require this 2-stage solution process as its domain of convergence is larger, thus saving much time.

6   Optimal Walking Experiments

Two main categorizations can be made in that we explore first walking without any form of lift propulsion. We then add to our biped the possibility of introducing an instantaneous impulsive force at the moment of liftoff to help the body move forward. In both settings, the additional effect of using ankle torques is investigated so that we compare all together 4 distinct cases. Liftoff impulses and ankle torques both help compensate for the absence of a foot in our biped model.

6.1   Optimal Forward Velocities vs. Energy

When energy is considered in terms of $(cal/kg/m)$, as in Section 4 then the equation

$$E_m = \frac{32}{v} + 0.005\,v \qquad (6)$$

has been shown experimentally to roughly model the relationship witnessed in humans between required energy E_m and the average forward walking velocity v [10]. This hyperbolic relationship has an energy minimizing walking velocity of 80 m/min. **Figure 3** displays the relationship that we encounter in our experiments which, while reasonably hyperbolic, has a much lower energy minimizing velocity of approximately 12 m/min. A possible conjecture for the disparity with optimal human walking is the lack of the foot effect which provides essentially an extension of the leg when the back heel lifts off of the ground propelling the body forward and reducing the effects of collision.

Figure 3 also compares optimal walking with and without impulsive liftoff forces. The dashdot and dotted lines in indicate the energy relationship for walking with an impulsive liftoff force. A significant energy savings is obtained over walking without such a liftoff force (solid and dashed lines), though there is no noticeable change to the optimal walking speed. The effect of ankle torques, which is also displayed, is small.
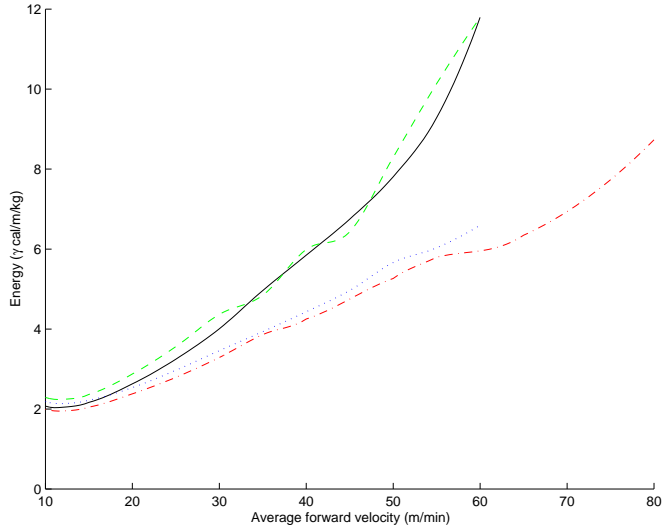
Figure 3: Required energy as a function of avg. forward velocity. With ankle torques (solid); no ankle torques (dashed); with ankle torques and liftoff force (dashdot); with liftoff force (dotted).
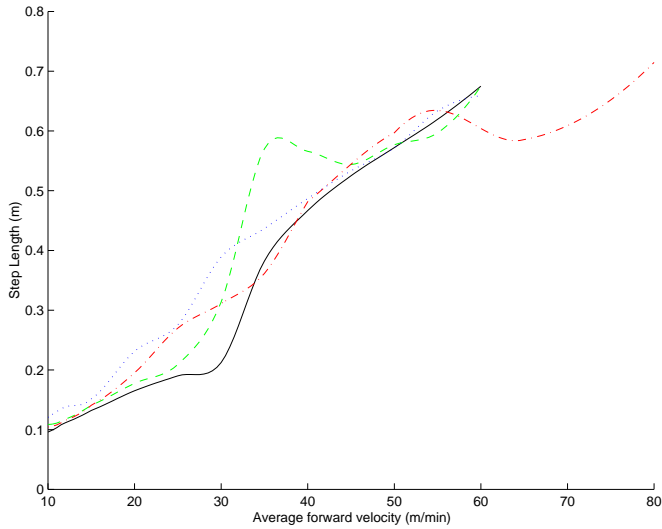

Figure 4: Optimal Step length as a function of average forward velocity. With ankle torques (solid); no ankle torques (dashed); with ankle torques and liftoff force (dashdot); with liftoff force (dotted).

6.2   Optimal Forward Velocities vs. Step Length

Corresponding to our 12 m/min globally optimal walk is also a much smaller step size of $0.1m$ than the $0.75m$ witnessed in humans. **Figure 4** also displays how the optimal size of the step increases with increasing average forward velocity; note that all cases yield a roughly linear relationship. The overall trend we observed is very similar to the standard observation that [10] optimal step length for human is directly proportional to the average forward velocity.
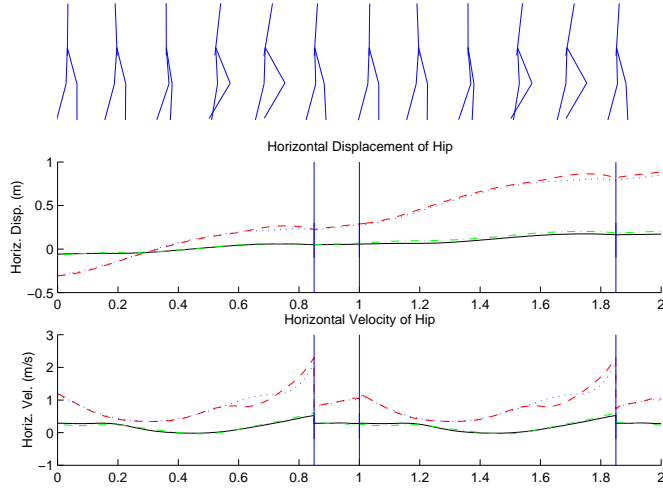
11

Figure 5: Optimal trajectories of hip horizontal position and velocity for walking with liftoff forces. Walk Speed: 12 m/min. No ankle torques (dashed); with ankle torques (solid). Walk Speed: 50 m/min. No ankle torques (dotted); with ankle torques (dashdot).
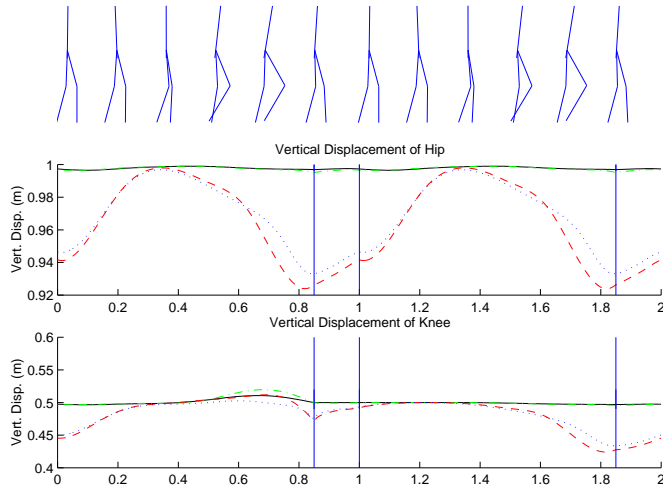

Figure 6: Optimal trajectories of hip and knee vertical positions for walking with liftoff forces. Walk Speed: 12 m/min. No ankle torques (dashed); with ankle torques (solid). Walk Speed: 50 m/min. No ankle torques (dotted); with ankle torques (dashdot).

Since the biped has no foot, how step length should be compared to that of a human is not clear.

6.3 Forward Velocities and Collisions

We display in **Figure 5** the hip horizontal displacement and hip forward velocity for a complete, periodic, double step with an impulsive liftoff force. In order that the various walking trajectories may be more easily compared, we plot on the horizontal axis the normalized time

for a step (normalized so that the final time for every step is 1). The stick walking figures on the top portion of the figure indicate for the two plots beneath it which part of the walking step the plotted points correspond to. The plots begin with the swing leg leaving the ground, and ends with the same leg about to leave the ground once again.

The solid (with ankle torques) and dashed (without ankles) lines indicate optimal walking solutions. The dashdot (with ankles) and dotted (without ankles) have an additional parameter fixed which is that of the average forward velocity set at a much faster 50 m/min. The first vertical line indicates the moment of collision, the second line is the time when the second step begins with the other leg lifting off the ground, and the last line is once again a collision of the swing leg with the ground.

From the velocity plot at the bottom of **Figure 5** we see the biped loses a considerable amount of forward velocity at the moment of collision, in particular for the faster walking speed. The faster walking speed serves to exaggerate the overall effects as it is also more apparent that the biped needs to slow down quite a bit near the middle of the swing phase rather being able to maintain a more constant forward velocity. With the inclusion of a liftoff force, our experiments have shown that we are able to obtain more consistent forward motion and the large variation evident in the velocity plot is substantially reduced over the case when liftoff forces are not included. We speculate that without the explicit modeling of the foot, the biped cannot efficiently operate at higher speeds.

We may observe the vertical movement of the hip and knee in **Figure 6**. The height of the hip and knees stays roughly at the same level during the slower $12\,m/min$ globally optimal walk while during faster walks, the well-known sinusoidal motion effect of the hip is more apparent [10].

6.4   Walking with and without Liftoff Forces

Figures 7 and 8 display the optimal applied torques for the model with and without impulsive liftoff forces from the same set of experiments as the previous section. Including an impulsive liftoff force is an easy way of modeling the same effects as having a foot. The solid and dashed lines indicate the torques for the optimal walking motion for the model with and without ankle actuation respectively. There is a notable difference between the 12 m/min (globally optimal) and the 50 m/min walk. It is evident that the torques for the faster walk reach the magnitude constraints placed upon them several times. The torque saturations can be greatly reduced with the introduction of an impulsive liftoff force. These torques (and their rates) are of much smaller magnitude showing the beneficial effect this additional control parameter has.

For a given velocity, it is difficult to distinguish the difference between including and not including ankle actuation. The difference only becomes visible at the higher forward velocity when during the second phase a slightly smoother and smaller torque actuation is required for the hip and knee. An interesting effect witnessed in our experiments is that the knee comes more into use with ankle actuation. As a result, the torque inputs and associated cost in injected energy will be more equally distributed through the different joints of the biped.

7   Conclusion

Our investigation into the generation of minimum energy symmetric, periodic gaits gathers together several different research areas in the modeling and control of complex, nonlinear systems. Our ability to solve this problem has relied upon the use of recursive, symbolic multibody algorithms coupled with powerful numerical optimal control software. Some of the more interesting conclusions that can be made from our experiments are:
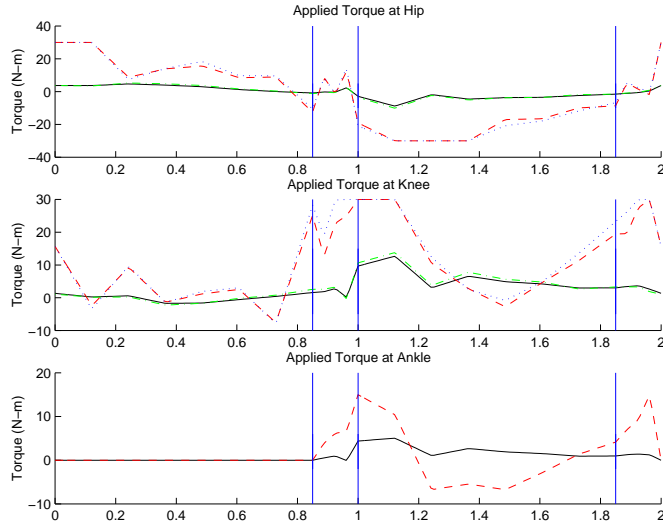
Figure 7: Optimal applied torques for walking without liftoff forces. Walk Speed: 12 m/min. No ankle torques (dashed); with ankle torques (solid). Walk Speed: 50 m/min. No ankle torques (dotted); with ankle torques (dashdot).
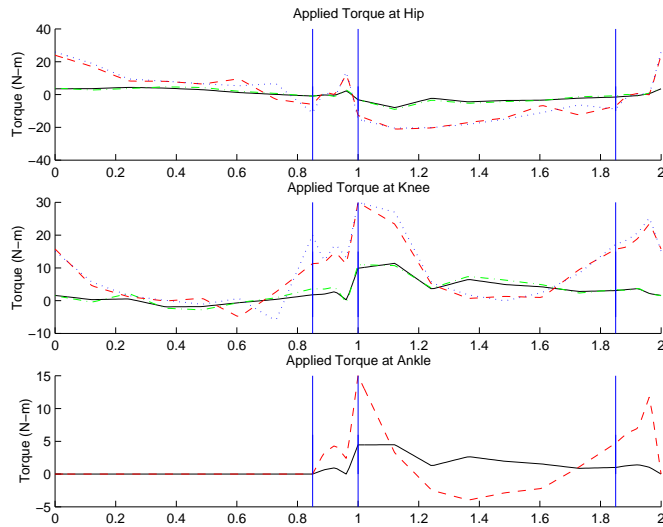

Figure 8: Optimal applied torques for walking with liftoff forces. Walk Speed: 12 m/min. No ankle torques (dashed); with ankle torques (solid). Walk Speed: 50 m/min. No ankle torques (dotted); with ankle torques (dashdot).

- Minimum energy walk for biped model (without explicit modeling of the feet) has a much slower walk than optimal human walk.

- The optimal model walk has shorter steps than optimal human walk, however the notion of step length is problematical since the model has no feet.

14

- Impulsive liftoff forces help prevent torque saturation, smooth the walking motion, and reduce the energy consumed.

- Ankle actuation smooths the walking step and distributes the input torques more equally among the hip, the knee, and the ankle.

- Using polar coordinates as in Section 3.5 to convert leg vs hip geometric constraints to box constraints was critical to numerical success.

1 Appendix: Contact and Collision Algorithms

We give now a brief summary of the **Contact** and **Collision Algorithms**. If the tip contact constraint (free foot touching the ground) is given holonomically as $c(\theta) = 0$, then by taking time derivatives we also obtain

$$J_c\dot{\theta} = 0 \tag{7}$$
$$J_c\ddot{\theta} + \dot{J}_c\dot{\theta} = 0 . \tag{8}$$

where $J_c = \partial c/\partial\theta$. Multiplying (1) by J_c and substituting for $J_c\ddot{\theta}$ using (8), one obtains an operator expression for f_c.

$$
\begin{aligned}
f_c &= (J_c\mathcal{M}^{-1}J_c^T)^{-1}[-J_c\mathcal{M}^{-1}(u - \mathcal{C} - \mathcal{G}) - \dot{J}_c\dot{\theta}] \\
&= -\Lambda(J_c\ddot{\theta}_f + \dot{J}_c\dot{\theta}) , \\
&= -\Lambda Q\dot{V}_c .
\end{aligned}
\tag{9}
$$

$\Lambda^{-1} = (J_c\mathcal{M}^{-1}J_c^T)$ is a square matrix of dimension equal to the number of constraints, and it is a quantity related to the Khatib operational space inertia. $\ddot{\theta}_f$ are the free generalized accelerations without the influence of the contact force in the dynamics. The final expression for f_c is expressed in terms of the constrained components of the spatial acceleration $\dot{V}_c$, where $Q\dot{V}_c = d/dt(QV_c) = d/dt(J_c\dot{\theta})$. The quantity V_c likewise is composed of the constrained components of the linear and angular velocities for the various links in the multibody system.

The true angle accelerations are the sum of $\ddot{\theta}_f$ and a correction term $\ddot{\theta}_\delta$ which results from the contact forces propagating throughout the body. These correction accelerations can be calculated from f_c by the relationship

$$\ddot{\theta}_\delta = \mathcal{M}^{-1}J_c^T f_c . \tag{10}$$

A very similar algorithm exists for calculating the change in velocities due to an inelastic collision with the ground. The change in the generalized velocities will depend on the leg tip velocities at the moment of contact with the ground, QV_c. One solves for the impulse force f_{imp},

$$f_{imp} = -\Lambda QV_c . \tag{11}$$

One may solve for $\dot{\theta}_\delta$ in $\dot{\theta}_\delta = \mathcal{M}^{-1}J_c^T f_{imp}$ to obtain the generalized velocities after collision $\dot{\theta}_+ = \dot{\theta}_- + \dot{\theta}_\delta$. The **Contact** and **Collision Algorithms** are discussed at greater length in [1], while recursive algorithms for the explicit calculation of the previously defined quantities in general tree-structured multibody systems are presented in [6].

2   Appendix: Reduced Dynamics Algorithm

With the introduction of holonomic constraints, such as the contact of legs with the ground, it is possible to construct a set of reduced unconstrained dynamics of dimension equal to the number of degrees of freedom, N, minus the number of constraints, m. In this section, we outline our approach to calculating the independent generalized accelerations of the reduced set of dynamics. The novelty of this approach is that it does not require the explicit construction of the reduced dynamics. It will be shown how one may extract the solution of the reduced dynamics from the solution of the Contact Algorithm and the solution of the forward dynamics of the entire system. One main advantage of using a reduced unconstrained dynamical model is that optimization programs which require integration of the dynamics will encounter less numerical difficulties.

In order to satisfy the constraint condition (7), the generalized velocities $\dot{\theta}$ must belong to the null space of the constraint Jacobian, $\mathcal{N}(J_c) \subset R^{N-m}$. If the columns of X represents a basis for $\mathcal{N}(J_c)$, then there exists a representation of $\dot{\theta}$ with respect to X denoted here by ξ, $\dot{\theta} = X\xi$. Substituting $\ddot{\theta} = X\dot{\xi} + \dot{X}\xi$ into the dynamical equations and multiplying on the left by X^T will give us the reduced dynamics,

$$\mathcal{M}_\xi \dot{\xi} + \mathcal{C}_\xi + \mathcal{G}_\xi = u_\xi \, , \tag{12}$$

where $\mathcal{M}_\xi = X^T \mathcal{M} X$, $\mathcal{C}_\xi = X^T \mathcal{M} \dot{X} \xi + X^T \mathcal{C}$, $\mathcal{G}_\xi = X^T \mathcal{G}$, and $u_\xi = X^T u$.

If θ represents the generalized coordinates of the system, then it is possible to choose $N - m$ independent coordinates θ_1 and m dependent coordinates θ_2 such that $J_{c,1} \dot{\theta}_1 + J_{c,2} \dot{\theta}_2 = 0$ may be used as an alternative expression for (7). This approach was made in [12], and it leads to an obvious choice for X,

$$\dot{\theta} = X\xi = X_0 \dot{\theta}_1 = \begin{bmatrix} I \\ -J_{c,2}^{-1} J_{c,1} \end{bmatrix} \dot{\theta}_1 \, . \tag{13}$$

An advantage of making this choice for the basis X is that, as will be shown in the **Reduced Dynamics Algorithm**, the reduced accelerations are simply represented as $\dot{\xi} = \ddot{\theta}_1$. Our goal here is to show that the solution of the contact algorithm may be used to obtain a solution of the reduced forward dynamics problem. Then an optimization routine performing numerical integration need only integrate on the independent coordinates $\ddot{\theta}_1$. We first give a lemma before the algorithm is presented.

Lemma 1 *Let X be a basis for the null space of the constraint Jacobian, $\mathcal{N}(J_c)$, and assume that at time $t = 0$, the state $(\theta, \dot{\theta})$ satisfies the constraint conditions $c(\theta(0)) = 0$, $J_c \dot{\theta}(0) = 0$. Then the following statements are equivalent:*

(a) $\dot{\theta}$ and $\ddot{\theta}$ satisfy $J_c \ddot{\theta} + \dot{J}_c \dot{\theta} = 0$.

(b) There exists an $N - m$ dimensional vector ξ which satisfies $\dot{\theta} = X\xi$.

(c) $X\dot{\xi} = \ddot{\theta} - \dot{X}\xi$ is consistent and has a unique solution $\dot{\xi}$.

Proof: $(c) \Rightarrow (a)$ Since X is a basis for $\mathcal{N}(J_c)$, then $J_c X \xi = 0$ and $d/dt(J_c X \xi) = 0$. So,

$$J_c \ddot{\theta} + \dot{J}_c \dot{\theta} = J_c X \dot{\xi} + (J_c \dot{X} + \dot{J}_c X)\xi = 0 \, .$$

$(a) \Rightarrow (b)$ Integrating (a) implies $J_c \dot{\theta} = 0$ since $J_c \dot{\theta}(0) = 0$ at time $t = 0$. $J_c \dot{\theta} = 0$ further implies that there exists a representation ξ for $\dot{\theta}$ with respect to X, $\dot{\theta} = X\xi$. $(b) \Rightarrow (c)$ Differentiating $\dot{\theta} = X\xi$ and observing that X is full rank gives the desired result.
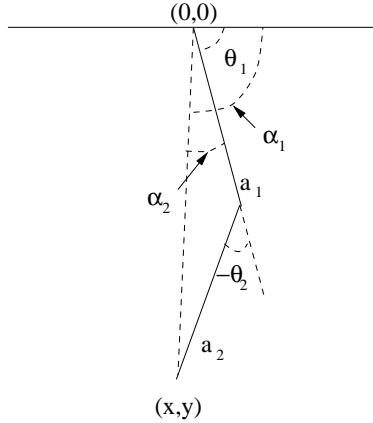**Reduced Dynamics Algorithm**

16

Figure 9: Inverse Kinematics Problem for 2-link Leg the bottom (x, y) is the foot fixed on the ground, while the top $(0, 0)$ is the hip

1. Beginning with an independent set of coordinates $\xi = \theta_1$, solve via inverse kinematics for θ_2 from θ_1. Similarly solve for $\dot{\theta}_2$ from $\dot{\theta}_1$ using the algebraic relation $\dot{\theta}_2 = -J_{c,2}^{-1} J_{c,1} \dot{\theta}_1$.

2. Given a set of torque inputs u, one may solve for $\ddot{\theta}$ with the contact algorithm. Simple algebraic manipulation shows that this solution satisfies (a) of Lemma 1.

3. Using Equation (13), it follows that $\dot{\xi} = \ddot{\theta}_1$, and it satisfies the reduced dynamics (12).

This algorithm thus yields the reduced forward dynamics mapping $u \rightarrow (\xi, \dot{\xi})$.

3 Appendix: Reduced Dynamics for the Biped

A key component of our dynamical modeling of the biped is the use of the Reduced Dynamics Algorithm presented in Section 2 of the Appendix. We have already mentioned that because of the contact constraints in phase one and in phase two of walking, we are faced with a differential-algebraic system. Two courses of actions are possible when it is necessary to integrate the dynamics, one being the use of specially tailored integration routines which often require the partial derivatives of the various contact constraints. The preferable approach, however, is to use a reduced unconstrained set of dynamics which evolve on the constraint manifold. Then it is possible to use standard integration procedures.

Recall that one of the primary difficulties of the Reduced Dynamics Algorithms is that the inverse kinematics must be used to solve for the dependent states. For the biped, the first task is to solve for the angle which determines the position of each leg. This is easy since our problem is equivalent to solving for the joint angles of a 2-link manipulator when its endpoints are known.

The following well-known solution comes from Spong and Vidyasagar [13]. In Figure 9 is displayed the inverse kinematics problem. Let θ_1 and θ_2 be the desired joint angles, a_1 and a_2 the lengths of the upper and lower legs respectively, and α_1 and α_2 two intermediate angles. We assume that one end of the 2-link arm has been transferred to the origin while the other end has coordinates (x, y). From the Law of Cosines,

$$D = \cos(\theta_2) = \frac{x^2 + y^2 - a_1^2 - a_2^2}{2 a_1 a_2} \ . \tag{14}$$

17

Also, $\sin(\theta_2) = \pm\sqrt{1 - D^2}$. In our case, since the knees only bend in one direction, the minus sign is always used so that

$$\theta_2 = \tan^{-1} \frac{-\sqrt{1 - D^2}}{D} \ . \tag{15}$$

Now θ_1 may be obtained easily from two intermediate angles α_1 and α_2. Let the angle $\alpha_1 = \tan^{-1}(y/x)$ while $\alpha_2 = \tan^{-1}\left(\frac{a_2 \sin\theta_2}{a_1 + a_2 \cos\theta_2}\right)$. The final expression for θ_1 is

$$\theta_1 = \tan^{-1}(y/x) - \tan^{-1}\left(\frac{a_2 \sin\theta_2}{a_1 + a_2 \cos\theta_2}\right) \ . \tag{16}$$

The dependent position states then are $x_7 = \theta_1 - x_1$ and $x_9 = \theta_2$.

Now we turn to computing the *velocities* along the manipulator. The velocities are known at both ends of the 2-link manipulator, so the Collision Algorithm can be used to give the joint velocities uniquely. This is done by initializing the algorithm for a 2-link manipulator with the known spatial velocity at the joint connecting the upper leg and the torso. The joint angles have been previously calculated and the joint velocities are arbitrary as there will only be one solution. The updated velocities will then correspond to the values of the states x_8 and x_{10}.

References

1. D. Agahi and K. Kreutz-Delgado (1994) A star topology dynamic model for efficient simulation of multilimbed robotic systems , In *IEEE International Conf. on Robotics and Automation* , pages 352–7.
2. C.K. Chow and D.H. Jacobson (1971) Studies of Human Locomotion via Optimal Programming , In *Math. Biosciences* , volume 10, pages 239–306.
3. P.E. Gill, W. Murray, M.A. Saunders, M.H. Wright User's Guide for NPSOL 5.0 .
4. P.E. Gill, W. Murray, and M.A. Saunders (1997) SNOPT: An SQP algorithm for large-scale constrained optimization , In *Num. Anal. Rep, Rep. 97-2* , Dept. of Math., UCSD, La Jolla, CA.
5. A. Goswami, B. Espiau, and A. Keramane (1997) Limit Cycles in a Passive Compass Gait Biped and Passivity-Mimicking Control Laws , In *Autonomous Robots* , volume 4, pages 273–286.
6. M. Hardt (1999) Multibody Dynamical Algorithms, Numerical Optimal Control, with Detailed Studies in the Control of Jet Engine Compressors and Biped Walking , Ph.D. Thesis, Elec. Eng., UCSD, La Jolla, CA.
7. M. Hardt, K. Kreutz-Delgado, and J. William Helton (1998) Minimal Energy Control of a Biped Robot with Numerical Methods and a Recursive Symbolic Dynamic Model , In *37th IEEE Conf. on Decision and Control* , pages 413–6.
8. S. Kajita and K. Tani (1996) Experimental Study of Biped Dynamic Walking , In *IEEE Control Systems* , pages 13–19.
9. T. McGeer (1990) Passive Dynamic Walking , In *The International Journal of Robotics Research* , volume 9(2), pages 62–82.
10. J. Rose and J.G. Grimble (1994) Human Walking , Williams & Wilkins.
11. L. Roussel, C. Canudas de Wit, and A. Goswami (1998) Generation of Energy Optimal Complete Gait Cycles for Biped Robots , In *1998 IEEE International Conf. on Robotics & Automation* , pages 2036–41.
12. C.L. Shih and W. Gruver (1992) Control of a Biped Robot in the Double-Support Phase , In *IEEE Trans. on Systems, Man, and Cybernetics* , volume 22(4), pages 729–35.

13. M.W. Spong and M. Vidyasagar (1989) Robot Dynamics and Control , John Wiley & Sons.
14. O. von Stryk (1999) User's Guide for DIRCOL 2.0. A direct collocation method for the numerical solution of optimal control problems .
15. O. von Stryk (1993) Numerical Solution of Optimal Control Problems by Direct Collocation , In *R. Bulirsch, A. Miele, J. Stoer, K.-H. Well (eds.):* Optimal Control, *Int'l Ser. in Numerical Math.* , Birkhäuser, volume 111, pages 129–143.
16. O. von Stryk (1995) Numerische Lösung optimaler Steuerungsprobleme: Diskretisierung, Parameteroptimierung und Berechnung der adjungierten Variablen , Fortschritt-Berichte VDI, Reihe 8, Nr. 441, VDI-Verlag, Düsseldorf.